

Parametric Nonlinear Lumped Element Model for Circular CMUTs in Collapsed Mode

Elif Aydoğdu, *Student Member, IEEE*, Alper Ozgurluk, *Student Member, IEEE*,
Abdullah Atalar, *Fellow, IEEE*, and Hayrettin Köymen, *Senior Member, IEEE*

Abstract—We present a parametric equivalent circuit model for a circular CMUT in collapsed mode. First, we calculate the collapsed membrane deflection, utilizing the exact electrical force distribution in the analytical formulation of membrane deflection. Then we develop a lumped element model of collapsed membrane operation. The radiation impedance for collapsed mode is also included in the model. The model is merged with the uncollapsed mode model to obtain a simulation tool that handles all CMUT behavior, in transmit or receive. Large- and small-signal operation of a single CMUT can be fully simulated for any excitation regime. The results are in good agreement with FEM simulations.

I. INTRODUCTION

ACCURATE modeling of capacitive micromachined ultrasonic transducers (CMUTs) is essential to reach a successful design without trial and error. Because a CMUT's mechanical operation is distributed and nonlinear, its modeling is not straightforward. There have been several approaches reported in the literature. The most reliable, and very commonly used, method has been finite element modeling (FEM) [1]–[3]. In the finite element analysis environment, the operation of a CMUT membrane can be simulated with high accuracy at the cost of extensive computation and time consumption. This computation cost forces researchers to use alternative methods for predicting CMUT operation. These methods include characterization of CMUT behavior using experimental observations [4]–[6], analytical calculation of the distributed membrane bending and the electrical-mechanical energy transfer efficiency [7]–[10], and defining lumped elements to develop models suitable for dynamic simulations. Electrical circuit elements constitute a convenient basis for lumped element modeling. Starting from Mason's model for acoustic transducers [11], equivalent circuit modeling has been improving as a powerful alternative to FEM [9], [12]–[15], especially for array modeling [16]–[18]. The studies directed toward understanding and modeling mutual impedance of CMUT arrays [2], [4], [17], [19], [20]

have helped to improve the accuracy of lumped element simulations.

CMUTs are commonly used in large arrays. The operation of large CMUT arrays can only be predicted using lumped element modeling, because the computation cost of FEM exponentially increases with increasing cell count. Currently, the uncollapsed-mode operation of CMUT arrays is well understood through equivalent circuit model simulations [17]. The mechanical and electrical properties of uncollapsed-mode operation are perfectly adapted to the lumped model [21].

On the other hand, the collapsed-mode operation has not been completely modeled so far, because it has not been possible to obtain an analytical expression for the collapsed membrane bending.

Collapsed mode offers high coupling efficiency, as shown in [22]. In [23], it was observed that a CMUT can produce higher transmit power in collapsed mode than in uncollapsed mode. To explore this mode further, and perform array simulations, it is necessary to obtain a lumped element model. An equivalent circuit model for collapsed mode was previously introduced in [24]; however, it was not a fully parametric model. Numerical calculations of the bending profile of a specific CMUT design were adapted to the model; hence, new numerical calculations had to be carried out for every new set of design parameters. Also, the bending profile calculations were done utilizing Timoshenko's [25] uniform force solution, and this uniformity approximation did not result in high accuracy.

In this work, a fully parametric model for a CMUT in collapsed mode is obtained. First, the collapsed membrane bending is calculated with high accuracy, utilizing the nonuniform electrostatic force expression in Timoshenko's equation instead of the uniform force approximation. The calculations are then adapted to the lumped element model of [21]. We model the collapsed-mode operation of a single CMUT at FEM accuracy, including the self-radiation impedance of collapsed mode [26]. We also merge the model with the uncollapsed mode part given in [18] and obtain a single model for the entire large-signal operation of the CMUT.

II. CALCULATION OF BENDING PROFILE IN COLLAPSED MODE

Fig. 1 shows a CMUT cell in the collapsed mode; Table I lists the description of relevant variables.

Manuscript received July 1, 2013; accepted September 18, 2013. This work was supported by the Scientific and Technological Research Council of Turkey (TUBITAK) under project grant 110E216. A. Atalar acknowledges the support of the Turkish Academy of Sciences (TUBA).

E. Aydoğdu, A. Atalar, and H. Köymen are with the Electrical and Electronics Engineering Department, Bilkent University, Ankara, Turkey (e-mail: elifaydogdu@gmail.com).

A. Ozgurluk is with the Electrical Engineering and Computer Sciences Department, University of California, Berkeley, Berkeley, CA.

DOI <http://dx.doi.org/10.1109/TUFFC.2014.2888>

TABLE I. DESCRIPTION OF PARAMETERS.

a	Membrane radius
b	Contact radius in case of collapse
$x(r)$	Displacement profile
ε_0	Dielectric permittivity of air
ε_r	Relative dielectric permittivity of insulator
t_g	Gap height
t_i	Insulator thickness
t_{ge}	Effective gap height: $t_{ge} = t_g + t_i/\varepsilon_r$
t_m	Membrane thickness
E	Young's modulus of membrane material
ν	Poisson's ratio of membrane material
ρ	Density of membrane material
D	Flexural rigidity of membrane material
ρ_0	Density of immersion medium
c_0	Speed of sound in immersion medium

A. Accurate Formulation of Deflection-Force Relation

Timoshenko [25] provides the formulation for the bending profile $x(r)$ for a circularly symmetrical pressure distribution $P(r)$ on a circular plate as

$$r \frac{d}{dr} \left(\frac{1}{r} \frac{d}{dr} \left(r \frac{d}{dr} x(r) \right) \right) = \frac{1}{D} \int_b^r P(\xi) \xi d\xi, \quad (1)$$

where r is the radial variable, and $D = Et_m^3/12(1 - \nu^2)$.

A convenient approach for calculation of uncollapsed membrane bending is to approximate all forces with an equivalent uniform pressure distribution across the membrane. This way, $x(r)$ can be expressed analytically and can also be used to obtain analytical expressions for lumped electrical force, capacitance, and mechanical compliance.

On the other hand, this uniform pressure approximation does not yield accurate results for a collapsed membrane, because the electrical force distribution is highly nonuniform in collapsed mode. In previous studies [24], it was observed that the calculated contact radius turns out to be smaller than expected when the force distribution on the membrane is assumed to be uniform. In reality, the electrical force increases significantly close to the contact point because of the decreased gap, exerting a higher pulling force in this region compared with the periphery.

We utilize the real force distribution, which we call the model force, in Timoshenko's equation:

$$r \frac{d}{dr} \left(\frac{1}{r} \frac{d}{dr} \left(r \frac{d}{dr} x(r) \right) \right) = \frac{1}{D} \int_b^r \left(P_b + \frac{\varepsilon_0 V^2}{2(t_{ge} - x(\xi))^2} \right) \xi d\xi. \quad (2)$$

Here, the pressure term $P(r)$ is replaced with the electrical force density at every point on the membrane, added to the remaining uniformly distributed static pressure P_b . P_b accounts for the ambient atmospheric or hydrostatic pressure. t_{ge} is the effective gap height, with $t_{ge} = t_g + t_i/\varepsilon_r$, where t_g is the gap height, t_i is the insulator thickness, and ε_r is the relative dielectric permittivity of the insulator, as given in Table I. The electrical force density

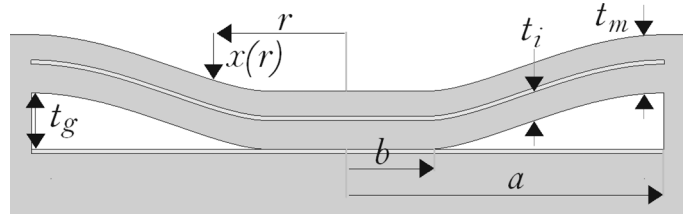


Fig. 1. The dimensional parameters of a CMUT in collapsed mode.

is the electrostatic force on the unit area capacitor with a gap $t_{ge} - x(r)$, having a voltage V across it.

There is no analytical solution for $x(r)$ of (2). We first normalize the variables and rearrange (2) into the generic form

$$\bar{r} \frac{d}{d\bar{r}} \left(\frac{1}{\bar{r}} \frac{d}{d\bar{r}} \left(\bar{r} \frac{d}{d\bar{r}} \bar{x}(\bar{r}) \right) \right) = \int_{\bar{b}}^{\bar{r}} 64 \left(\frac{P_b}{P_g} + \frac{2(V/V_r)^2}{9(1 - \bar{x}(\xi))^2} \right) \xi d\xi, \quad (3)$$

where the normalized variables are

$$\bar{r} = \frac{r}{a}, \quad \bar{b} = \frac{b}{a}, \quad \bar{x}(\cdot) = \frac{x(\cdot)}{t_{ge}}. \quad (4)$$

P_g is the pressure that corresponds to a peak membrane displacement of t_{ge} at zero bias ($\bar{x}(0) = 1$), and V_r is the collapse voltage at vacuum [21]:

$$P_g = \frac{64Dt_{ge}}{a^4}, \quad V_r = \frac{16}{3a^2} \sqrt{\frac{Dt_{ge}^3}{\varepsilon_0}}. \quad (5)$$

The boundary conditions of the differential equation in (3) can be written as

$$\begin{aligned} \bar{x}(\bar{r})|_{\bar{r}=1} &= 0, \quad \bar{x}(\bar{r})|_{\bar{r}=\bar{b}} = \frac{t_g}{t_{ge}}, \quad \frac{d}{d\bar{r}} \bar{x}(\bar{r})|_{\bar{r}=1} = 0, \\ \frac{d}{d\bar{r}} \bar{x}(\bar{r})|_{\bar{r}=\bar{b}} &= 0, \quad \frac{d^2}{d\bar{r}^2} \bar{x}(\bar{r})|_{\bar{r}=\bar{b}} = 0. \end{aligned} \quad (6)$$

The input parameters are V/V_r , P_b/P_g , and t_g/t_{ge} . The resulting \bar{b} and $\bar{x}(\bar{r})$ are calculated using the algorithm described in the next section.

B. Solution Algorithm

Our strategy of solving (3) under the boundary conditions of (6) is expressing the force term in such a way that an analytical solution can be obtained. If the pressure term can be expressed as a K th degree polynomial, as in

$$\bar{r} \frac{d}{d\bar{r}} \left(\frac{1}{\bar{r}} \frac{d}{d\bar{r}} \left(\bar{r} \frac{d}{d\bar{r}} \bar{x}(\bar{r}) \right) \right) = \int_{\bar{b}}^{\bar{r}} \left(\sum_{n=1}^K c_n \xi^n \right) d\xi, \quad (7)$$

an analytical solution exists:

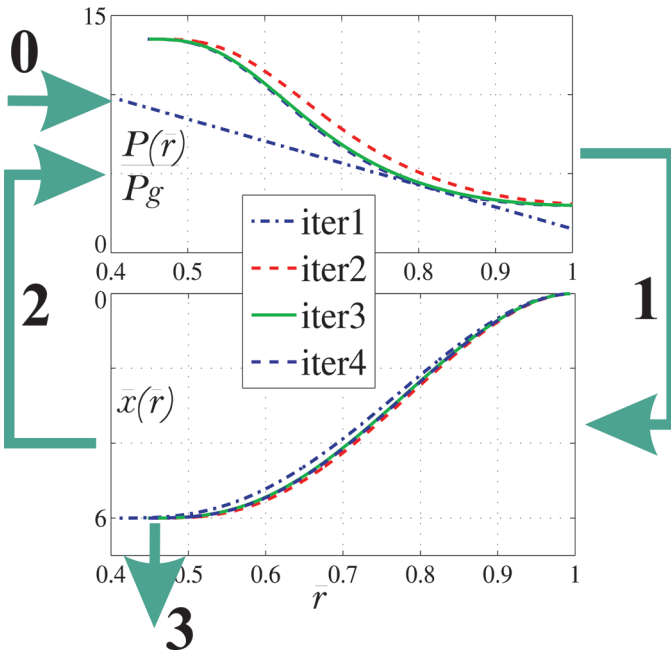


Fig. 2. Demonstration of iterative algorithm for solving $\bar{x}(\bar{r})$.

$$\bar{x}(\bar{r}) = A_1 + A_2 \bar{r}^2 + A_3 \log(\bar{r}) + A_4 \bar{r}^2 \log(\bar{r}) + \sum_{n=1}^K \frac{c_n \bar{r}^{n+3}}{(n+1)^2(n+3)^2} + \bar{r}^2(1 - \log(\bar{r})) \sum_{n=1}^K \frac{c_n \bar{b}^{n+1}}{4(n+1)}, \quad (8)$$

where A_1 , A_2 , A_3 , and A_4 are the constants of integration.

We use (8) in our iterative solution routine as shown in Fig. 2 and as follows:

- 0) Given the physical parameters, the normalized static force, and the excitation voltage, start with an initial guess of the pressure distribution. To enable faster convergence, the following linearly varying distribution is used as the initial guess:¹

$$\frac{P(\bar{r})}{P_g} = \frac{P_b}{P_g} + 1.5 \frac{2(V/V_r)^2(1 - \bar{r})}{9(1 - t_g/t_{ge})^2}.$$

- 1) A polynomial with coefficients c_n ($n = 0, 1, \dots, K$) is fitted to the pressure distribution. To achieve convergence in all cases, we set $K = 14$. Substituting this polynomial into (7), an analytical expression for $\bar{x}(\bar{r})$ in (8) with five unknowns (A_1 , A_2 , A_3 , A_4 , and \bar{b}) is obtained. The first four boundary conditions in (6) are solved with a symbolic math package to express A_i in terms of \bar{b} . Then, the last boundary condition is used to determine \bar{b} by finding the zero-crossing point.
- 2) Using the obtained bending profile, $\bar{x}(\bar{r})$, the new pressure distribution is calculated through the elec-

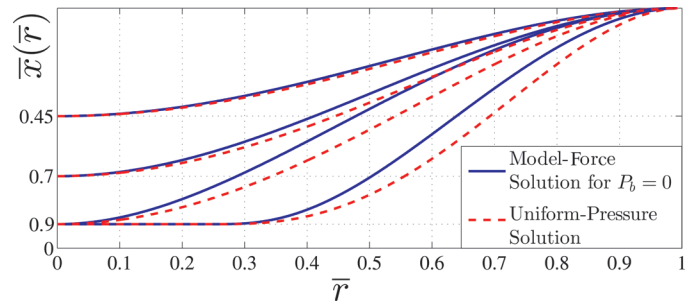


Fig. 3. Normalized deflection profiles of uniform pressure-loaded ($V = 0$) and model force-loaded ($P_b = 0$) membranes with $t_g/t_{ge} = 0.9$. Both profiles have the same peak displacements ($\bar{x}_P = 0.45$ and 0.7) in uncollapsed mode, and the same contact radius at snapback ($\bar{b} = 0$) and in collapsed mode ($\bar{b} = 0.25$).

trical force density expression in the right-hand side of (3):

$$\frac{P(\bar{r})}{P_g} = \frac{P_b}{P_g} + \frac{2(V/V_r)^2}{9(1 - \bar{x}(\bar{r}))^2}.$$

- 3) Go to step 1 and repeat until \bar{b} converges to a value within $\simeq 0.1\%$ difference between successive iterations.

Plots for $\bar{x}(\bar{r})$ calculations are given in Fig. 3, showing the difference between the bending profiles obtained with uniform pressure approximation, and model force with $P_b = 0$. There are four cases for a CMUT of $t_g/t_{ge} = 0.9$. In the uncollapsed mode, close to the collapse point, where $\bar{x}_P = \bar{x}(0) = 0.45$ (normalized peak displacement), the two profiles are very similar. This means that the uniform pressure approximation can be used for predicting uncollapsed-mode operation. However, as the displacement increases and the membrane enters the unstable region, the profiles start to diverge from each other, as seen in the $\bar{x}_P = 0.7$ plot. At the snapback point where the membrane barely touches bottom, and in the collapsed mode, the difference is even larger. At snapback, the uniform pressure approximation gives $V = 0.55 V_r$ and $\bar{x}_R = 0.402$ (normalized rms displacement),² whereas the model force results in $V = 0.58 V_r$ and $\bar{x}_R = 0.358$.

C. Results: Collapse and Snapback

The transduction force, capacitance, and compliance of a CMUT are determined by the deflection profile. The profile depends both on the normalized static pressure, which is uniformly distributed, and on the electrical force. In the model presented in this work, the effect of the profile is uniquely summarized in rms displacement. Although one can have the same rms displacement for different combinations of normalized static ambient pressure and electrical force, for a given pair of P_b/P_g and t_g/t_{ge} , electrical force

¹The initial pressure should be sufficiently high to make the membrane collapse.

²This is defined by $\bar{x}_R = \sqrt{1/(\pi a^2) \int_0^a 2\pi r \bar{x}^2(r) dr}$.

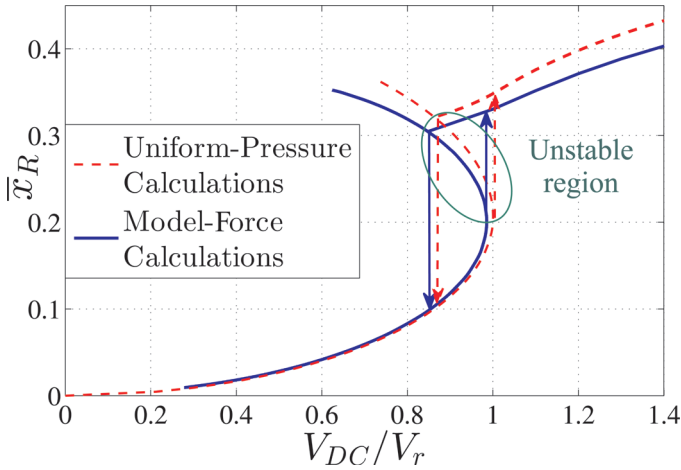


Fig. 4. Normalized displacement \bar{x}_R as a function of normalized applied voltage V_{DC}/V_r in uncollapsed and collapsed modes for $t_g/t_{ge} = 0.73$.

and the model elements can be uniquely defined as functions of rms displacement.

In Fig. 4, the normalized rms displacement ($\bar{x}_R = x_R/t_{ge}$) is plotted as a function of normalized bias voltage (V/V_r), similar to the CMUT biasing chart of [21]. The uncollapsed mode static analysis result for vacuum ($P_b = 0$), obtained with the uniform pressure approximation given in Fig. 5 of [21] is shown here with a dashed curve. The model force result shown in the plot (solid curve) is obtained also in vacuum, and the electrical force distribution on the membrane is highly nonuniform in the unstable region and in the collapsed region. Results obtained with the uniform pressure approximation of electrical force considerably diverge from the model force results in these regions. This is the source of the error in the prediction of snapback voltage in [24].

The transition from the uncollapsed mode to the collapsed mode happens at a voltage level where the membrane quickly passes through the unstable region and reaches a new balance point in the collapsed region (upward arrow). The snapback transition from the collapsed mode (at zero contact radius) to the uncollapsed mode occurs at a lower voltage (downward arrow).

III. LUMPED ELEMENT MODEL OF A SINGLE CMUT IN COLLAPSED MODE

The static calculations of collapsed membrane bending are used to define the elements in the lumped model of Fig. 5.

As seen from the electrical side, the CMUT behaves like a capacitor whose value depends on instantaneous membrane displacement. On the left side of Fig. 5, this is represented with C_0 , the undeflected membrane capacitance, and two current sources, i_C and i_V [21]

$$i_C = (C - C_0) \frac{dV(t)}{dt} \quad (9)$$

$$i_V = V(t) \frac{dC}{dt}, \quad (10)$$

where C is the instantaneous electrical capacitance.

In the electrical analogy of CMUT mechanics, the through and across variables are the rms velocity v_R and the corresponding energy-conserving rms force f_R [21]. On the right side of Fig. 5, we see the rms forces acting on the membrane: the electrical force f_R , the force resulting from ambient pressure F_{Rb} , and the dynamic external force f_{RI} .

The membrane exerts a restoring force determined by its compliance C_{Rm} . In the uncollapsed mode, the compliance has a fixed value [21] of

$$C_{Rm_0} = \frac{9(1 - v^2)a^2}{80\pi Et_m^2}. \quad (11)$$

The instantaneous values of C and C_{Rm} , and hence the transduction force, are determined by the instantaneous rms displacement. The static and instantaneous values are the same for each of these lumped model elements and force.

Because the through variable in the model is chosen as rms velocity, the model inductance, which conserves the energy, is the mass of the membrane [18], [21], [24]:

$$L_{Rm} = \pi a^2 t_m \rho. \quad (12)$$

The dynamic lumped element model is completed by terminating the acoustic port by appropriate radiation impedance [25]. The radiation impedance Z_{RR} is dependent on the instantaneous contact radius, and consequently on rms displacement.

A large set of static bending calculations is obtained to define the lumped parameters' dependence on x_R , t_g/t_{ge} , and P_b/P_g . For each bending profile solution, C is calculated first and it is used to find f_R and C_{Rm} .

Static analysis solutions for $\bar{x}(\bar{r})$ are obtained at seven different values of $t_g/t_{ge} = 0.4, 0.5, 0.6, 0.65, 0.73, 0.82$, and 0.9 , and interpolation can be done for intermediate values. When t_g/t_{ge} is less than 0.4 , the profile is the same as for uniform force distribution. When t_g/t_{ge} is chosen larger than 0.9 , the iterations do not converge; hence, the model is valid up to this value.

For each t_g/t_{ge} value, $P_b/P_g = 0, 0.2, 1$, and 2 cases are analyzed, because the intermediate values can be accu-

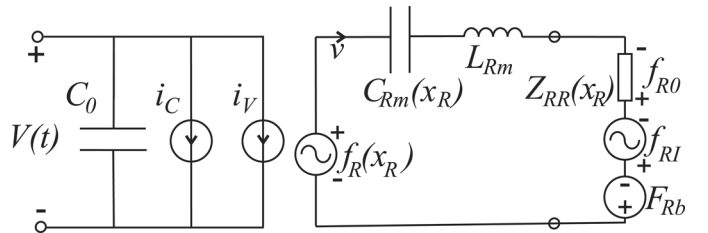


Fig. 5. The equivalent electrical circuit model of a CMUT with the through variable v_R .

rately interpolated from the data obtained at those static pressure levels.

For each case, solutions are obtained at 50 values of (V/V_r) between the normalized snapback voltage (the voltage level at which the membrane exits collapse mode) and a large value, 10. Therefore, a total of 1400 normalized cases are analyzed. With each sweep of (V/V_r) , keeping t_g/t_{ge} and P_b/P_g fixed, we obtained curves of C , C_{Rm} , and \bar{b} .

A. Capacitance

The capacitance C for a given deflection profile $\bar{x}(\bar{r})$ is

$$C = C_0 \int_0^1 \frac{2\bar{r}}{1 - \bar{x}(\bar{r})} d\bar{r} \quad (13)$$

$$C_0 = \varepsilon_0 \pi a^2 / t_{ge}. \quad (14)$$

In Fig. 6, the calculated C/C_0 values are plotted as a function of \bar{x}_R for different values of t_g/t_{ge} . For demonstration purposes, only the $P_b/P_g = 0.2$ case is given. When the membrane is uncollapsed, normalized capacitance is not affected by t_g/t_{ge} . In collapsed mode, the membrane can approach the substrate more for larger values of t_g/t_{ge} (thin insulator), and both the capacitance and the rms displacement can be comparatively large. As t_g/t_{ge} decreases (larger insulator thickness), both the displacement and the capacitance assume smaller values. The dashed line is the plot of uncollapsed mode capacitance calculated using the formula of uniform pressure approximation given in the Appendix. The collapsed mode calculations start with the snapback, so the initial points on solid lines correspond to the transition from collapsed mode to uncollapsed mode. However, those points do not coincide with the dashed plot because of the slight error caused by uniform pressure approximation.

B. Electrical Force

The electrical force is the energy-conserving force, defined as

$$f_R = \frac{dE_{el}}{dx_R} = \frac{V^2}{2} \frac{dC}{dx_R} = \frac{V^2}{2t_{ge}} \frac{dC}{d\bar{x}_R}. \quad (15)$$

The $dC/d\bar{x}_R$ term is introduced into the lumped model. With C/C_0 data in hand, $dC/d\bar{x}_R$ is numerically calculated for all t_g/t_{ge} and P_b/P_g . Capacitance and capacitance derivative are defined as separate functions of \bar{x}_R for every P_b/P_g and t_g/t_{ge} pair.³

³Observing that the P_b/P_g dependencies of capacitance and capacitance derivative are weak, it is possible to use the $P_b/P_g = 0.2$ data for all values of static pressure.

C. Compliance

The compliance of the membrane is defined as the ratio of x_R to the rms force on the membrane. In our deflection profile calculations, this force is the sum of the static electrical force F_R and the static uniform force F_{Rb} :

$$C_{Rm} = \frac{x_R}{F_R + F_{Rb}}. \quad (16)$$

Normalized compliance C_{Rm}/C_{Rm_0} is plotted with respect to \bar{x}_R in Fig. 7 for different t_g/t_{ge} values with $P_b/P_g = 0$. In the stable region of the uncollapsed mode, the membrane behaves like a linear spring of compliance C_{Rm_0} . In the unstable region of the uncollapsed mode, the compliance assumes higher values than C_{Rm_0} . When the membrane comes in contact with the bottom layer (this is also the snapback point), the compliance decreases nonlinearly with increasing displacement. The membrane becomes stiffer at larger contact radii. The point of contact is determined by the thickness of insulator. For the $t_g/t_{ge} = 0.4$ case, the insulator is so thick that the membrane touches the bottom layer without experiencing instability. On the other hand, for $t_g/t_{ge} = 0.9$, there is a wide region of instability at the end of which the compliance reaches a high value.

In Fig. 8, the normalized compliance is plotted for different levels of ambient pressure P_b/P_g (the $t_g/t_{ge} = 0.73$ case is shown). At vacuum, the membrane starts with zero deflection at $V = 0$, whereas there is an initial deflection for $P_b/P_g = 0.2, 1$ or 2 . For $P_b/P_g = 1$ or 2 , the ambient pressure is so large that the membrane touches bottom even at $V = 0$; hence it is always in collapse mode. For $P_b/P_g = 2$, the initial deflection is larger, and the initial compliance is correspondingly smaller. In the collapsed mode, the compliance at the same displacement turns out to be larger for higher ambient pressure.

D. Contact Radius

Fig. 9 shows the normalized contact radius, \bar{b} , as a function of \bar{x}_R for two values of P_b/P_g and for different values of t_g/t_{ge} . For $P_b/P_g = 1$, ambient pressure is strong enough to make the membrane touch the bottom layer

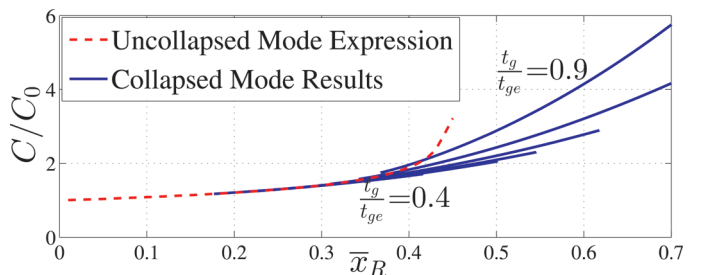


Fig. 6. Normalized electrical capacitance as a function of normalized rms displacement. $P_b/P_g = 0.2$ and $t_g/t_{ge} = 0.4, 0.5, 0.6, 0.65, 0.73, 0.82$, and 0.9 .

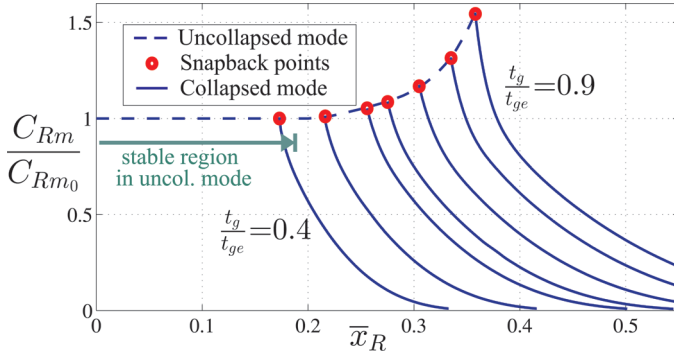


Fig. 7. Normalized compliance of the membrane as a function of normalized rms displacement. $P_b/P_g = 0$ and $t_g/t_{ge} = 0.4, 0.5, 0.6, 0.65, 0.73, 0.82$ and 0.9 .

even at zero voltage, so the $P_b/P_g = 1$ plots start at non-zero \bar{b} values.

We observe significant differences between the solid and dashed plots of the $t_g/t_{ge} = 0.9$ case. Close to snapback, they assume very different \bar{x}_R values at the same contact radius. This is because the bending profiles of uniform pressure-deflected and electrical force-deflected membranes are considerably different in collapsed mode.

To adapt all these calculations to the lumped model, polynomials are fitted to the numerical results of $C(\bar{x}_R)/C_0$, $dC(\bar{x}_R)/d\bar{x}_R$, $C_{Rm}(\bar{x}_R)/C_{Rm0}$, and $\bar{b}(\bar{x}_R)$. The polynomial coefficients are given in the Appendix.

E. Self-Radiation Impedance in Collapsed Mode

The interaction between the CMUT membrane and the radiation medium is determined by the velocity profile of the membrane. In uncollapsed mode, the entire membrane surface is active, whereas the periphery beyond the contact point is the active region in collapsed mode. The radiation impedance of this type of membrane is given in [26]:

$$Z_{RR} = \pi a^2 \rho_0 c_0 \{R_1(ka) + jX_1(ka)\}. \quad (17)$$

The real and imaginary parts of normalized radiation impedance are plotted in Fig. 10 as a function of ka (k is the

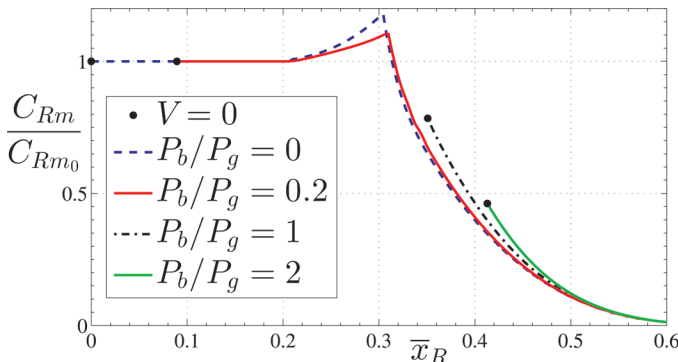


Fig. 8. Normalized compliance of the membrane as a function of normalized rms displacement for $t_g/t_{ge} = 0.73$ and $P_b/P_g = 0, 0.2, 1$ and 2 . Black dots show the initial displacements at $V = 0$.

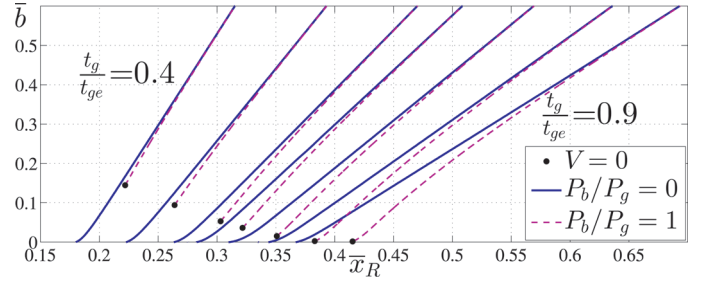


Fig. 9. Normalized contact radius as a function of normalized rms displacement for $P_b/P_g = 0, 1$, and $t_g/t_{ge} = 0.4, 0.5, 0.6, 0.65, 0.73, 0.82$, and 0.9 . $\bar{b} = 0$ corresponds to snapback point.

wavenumber) for different values of \bar{b} . Here, the $\bar{b} = 0$ curve is the same as the uncollapsed mode self-radiation impedance.

For the equivalent circuit model, we recorded those results at 13 values of contact radii, up to $\bar{b} = 0.6$. The required Z_{RR} value is interpolated dynamically in the contact radius space.

IV. COMPARISON OF LUMPED MODEL SIMULATIONS AND FEM ANALYSIS

The equivalent electrical circuit is simulated with a time-domain circuit simulator capable of handling frequency-domain input data.⁴ Parameter values used in the following simulations are given in Table II.

In Fig. 11, the positive and negative ramp signal response (in water) is given. The medium pressure is assumed to be zero. FEM⁵ simulations are added for comparison. The collapse timing is the same for both simulations, whereas there is a slight difference in snapback timing. According to the model, the snapback occurs at 31.5 V. FEM simulation predicts the snapback at 32 V. Because a single CMUT is considered, the radiation resistance is rather low and the membrane is lightly loaded. At the frequency of oscillation in uncollapsed mode, ka is small at about 0.2 and the approximate value of the radiation impedance Z_{RR} is $42.4 (1 + j10) \mu\text{N}\cdot\text{s}/\text{m}$. The quality factor of the radiation impedance is already about 10. The mass of the membrane increases this further. So, the bandwidth is quite small, and slowly decaying oscillations are observed after the sudden pull and release of the membrane.

In the collapsed mode, the resonance frequency is not fixed, because the membrane compliance decreases with increasing deflection. Fig. 12 depicts the resonance frequency, at which the maximum amount of real power is delivered to the medium, as a function of the dc bias voltage. Here, the CMUT of Table II is driven in water with an ac signal of 1 V peak voltage. The uncollapsed region

⁴Advanced Design System (Agilent Technologies Inc., Santa Clara, CA).

⁵FEM simulations are carried out in Ansys 13.0 (Ansys Inc., Canonsburg, PA). A 2-D axisymmetric model of a single CMUT is created as in [26].

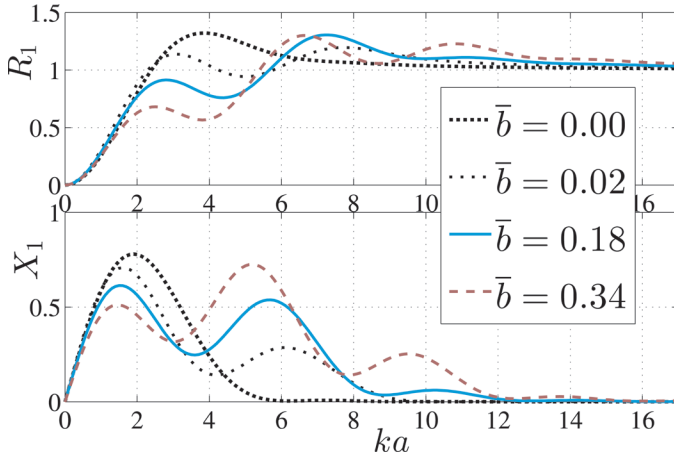


Fig. 10. The real (upper figure) and imaginary (lower figure) parts of self-radiation impedance of a CMUT in collapsed mode as a function of ka for various normalized contact radii, \bar{b} .

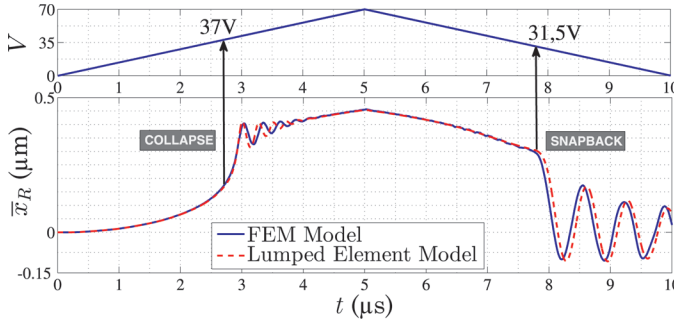


Fig. 11. The collapse and snapback behavior of the CMUT of Table II in water, predicted by lumped element and FEM simulations ($P_b = 0$).

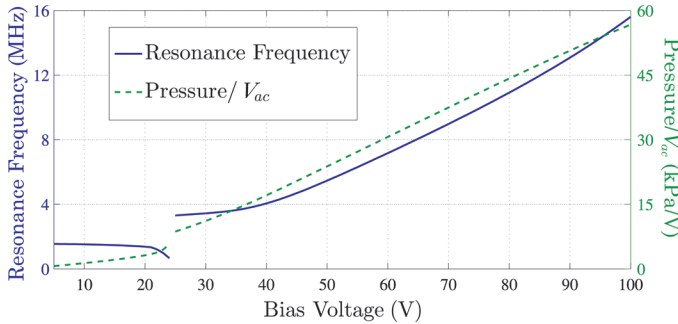


Fig. 12. The resonance frequency of a single CMUT (Table II, in water, $P_b = 1$ atm) and the pressure on the real part of the self-radiation impedance at the resonance frequency as a function of bias voltage, as predicted by the lumped element model.

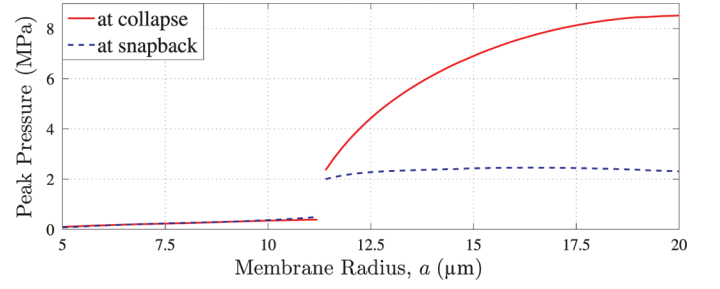


Fig. 13. The maximum instantaneous pressure at the membrane surface as a function of radius, at the rising (collapsing) and falling (snapback) edges of a 50 V pulse at ambient pressure in water.

is also plotted. As the bias voltage is increased toward the collapse voltage, the resonance frequency decreases slightly; but as soon as the membrane collapses, the membrane stiffening occurs, and the resonance frequency increases. As the collapse radius gets bigger, the membrane becomes even stiffer and the resonance frequency increases monotonically. The dashed line in the same figure shows the amplitude of the pressure on the medium radiation resistance at the corresponding resonance frequencies. Note that at a bias voltage of 100 V, the CMUT generates a pressure of more than 55 kPa/V.

As an application of the model, a CMUT cell in water at ambient pressure is driven with a 50 V pulse with 10 ns rise and fall times. The maximum instantaneous pressure across the membrane surface is plotted as a function of membrane radius a . The other dimensions of the CMUT cell are kept fixed at $t_m = 1 \mu\text{m}$, $t_i = 0.1 \mu\text{m}$, and $t_g = 0.1 \mu\text{m}$. The solid curve of Fig. 13 gives the maximum instantaneous pressure obtained at the rising edge of the voltage pulse (collapsing), and the dashed line gives the maximum pressure at the falling edge (at snapback).

As the radius of the membrane is increased, the collapse voltage decreases. For $a < 11.4 \mu\text{m}$, the collapse voltage is higher than 50 V; hence, collapse never occurs. The resulting pressure is relatively low. When $a > 11.4 \mu\text{m}$, collapse occurs on the rising edge. The pressure maximum increases almost 10 times. As a is increased further, the membrane is driven more and more in the deep-collapse mode. The pressure maximum at the rising edge increases monotonically as the cell radius is increased. This prediction is consistent with the measurement results of CMUTs in deep-collapse mode [23]. On the other hand, the pressure maximum at the falling edge seems to be saturated around a constant value.

V. CONCLUSION

In this work, the deflection profile of a circular CMUT in collapsed mode is numerically calculated by introducing a radially dependent electrical force into Timoshenko's equation. Using this force profile, the deflection and the snapback point are calculated precisely. A large set of numerical solutions is used to define the elements of the equivalent circuit model for the collapsed mode. The

TABLE II. PARAMETERS OF CMUT CELL USED IN SIMULATIONS.

E	110 GPa
ν	0.27
ϵ_r	5.4
ρ	3.1 g/cm ³
a	30 μm
t_m	1.2 μm
t_i	0.4 μm
t_g	0.2 μm

TABLE III. PARAMETER EXPRESSIONS IN UNCOLLAPSED AND COLLAPSED MODES.

Uncollapsed mode			Collapsed mode		
C_{Rm}	if $h_u(\bar{x}_R) < h_c(\bar{x}_R)$,	$= C_{Rm_0} h_u(\bar{x}_R)$, where $h_u(\bar{x}_R) = \begin{cases} \sum_{i=0}^4 l_i \bar{x}_R^i & \text{if } (\sum_{i=0}^4 l_i \bar{x}_R^i > 1) \\ 1 & \text{otherwise} \end{cases}$	else	$= C_{Rm_0} h_c(\bar{x}_R)$, where $h_c(\bar{x}_R) = \begin{cases} \sum_{i=0}^7 m_i \bar{x}_R^i & \text{if } (\sum_{i=0}^7 m_i \bar{x}_R^i > 0) \\ 0 & \text{otherwise} \end{cases}$	
C	if $\bar{x}_R < X_C$,	$= C_0 g(\sqrt{5}\bar{x}_R)$, $g(u) = \frac{\tanh^{-1}(\sqrt{u})}{\sqrt{u}}$	else	$= C_0 \sum_{i=0}^3 n_i \bar{x}_R^i$	
f_R	if $\bar{x}_R < X_f$,	$= \frac{\sqrt{5}V^2 C_0}{2t_{ge}} g'(\sqrt{5}\bar{x}_R)$, $g'(u) = \frac{1}{2u} \left(\frac{1}{1-u} - g(u) \right)$	else	$= \frac{V^2 C_0}{2t_{ge}} \sum_{i=1}^3 i n_i \bar{x}_R^{i-1}$	
b	if $\bar{x}_R < X_b$,	$= 0$	else	$= a \sum_{i=0}^6 p_i \bar{x}_R^i$	
Z_{RR}	if $\bar{b} = 0$,	$= Z(ka, \bar{b})$, with $\bar{b} = 0$	else	$= Z(ka, \bar{b})$, with $\bar{b} = 0.05, 0.1, 0.15, \dots, 0.6$	

TABLE IV. TABLE OF POLYNOMIAL COEFFICIENTS FOR $P_b/P_g = 0.2$ AND $t_g/t_{ge} = 0.73$.

l_0	l_1	l_2	l_3	l_4			
43.324	-54.67	330.07	-876.04	877.55			
m_0	m_1	m_2	m_3	m_4	m_5	m_6	m_7
537.77	-7978.88	50668.32	-177920.22	372639.41	-465350.30	320838.34	-94225.80
X_C	X_F	n_0	n_1	n_2	n_3		
0.2579	0.3045	1.1297	-0.8666	6.0994	-0.1124		
X_b	p_0	p_1	p_2	p_3	p_4	p_5	p_6
0.32	13.0537	-145.5684	625.2401	-1305.847	1349.5205	-552.4294	0

model is merged with the uncollapsed mode model. We can predict any large or small-signal operation of a single CMUT in the order of a minute. The effect of any parameter on the performance can be determined very quickly and the model can be used to optimize CMUT geometries for the highest transmit power, the best receive sensitivity, or the optimum driving voltage waveform.

Simulations with the model show that high transmit pressures can be achieved by operating in deep-collapse mode. As future work, we will introduce the mutual impedance of collapsed CMUTs to model arrays of collapsed mode CMUTs.

APPENDIX

Table III lists all the uncollapsed- and collapsed-mode expressions for lumped parameters, and the mode transition conditions. For the uncollapsed mode, we have nonlinear equations [21]. For the collapsed mode, we have polynomials for $t_g/t_{ge} = 0.4, 0.5, 0.6, 0.65, 0.73, 0.82$, and 0.9 , and $P_b/P_g = 0, 0.2, 1$, and 2 .

Continuous transition between collapsed and uncollapsed regions is ensured by defining the transition points exactly at the intersections of uncollapsed and collapsed mode expressions.

The coefficients of the polynomials and the transition points are provided in supplementary documents (Fig. 1). As an example, the $t_g/t_{ge} = 0.73$, $P_b/P_g = 0.2$ case is given in Table IV. Simulations at intermediate t_g/t_{ge} and P_b/P_g values can be performed using interpolation. For $t_g/t_{ge} = 0.58$ and $P_b/P_g = 0.4$, the instantaneous capacitance and compliance should be calculated as

$$C|_{t_g/t_{ge}=0.58} = 0.2C|_{t_g/t_{ge}=0.5} + 0.8C|_{t_g/t_{ge}=0.6}$$

$$C_{Rm}|_{P_b/P_g=0.4} = 0.75C_{Rm}|_{P_b/P_g=0.2} + 0.25C_{Rm}|_{P_b/P_g=1}$$

Polynomials are sensitive to coefficient precision, and the provided precision should be conserved when they are used in a model.

The normalized compliance is valid for $x_R/t_g < 0.8$, and the lumped model is not guaranteed to converge to a solution beyond this value.

The medium impedance is dependent on the frequency, and also on the contact radius in collapsed mode. Its value is introduced through lookup tables. There is a single lookup table for uncollapsed mode, whereas there are 12 lookup tables of collapsed mode for $\bar{b} = 0.05, 0.1, 0.15, 0.2, \dots, 0.55, 0.6$. Impedance at intermediate \bar{b} values should be interpolated. All of the lookup tables for $R_1(ka) + jX_1(ka)$ are given as s2p files in the supplementary document (Fig. 1). The frequency parameter corresponds to ka in all files.

REFERENCES

- [1] B. Bayram, G. G. Yaralioglu, M. Kupnik, A. S. Ergun, O. Oralcan, A. Nikoozadeh, and B. T. Khuri-Yakub, "Dynamic analysis of capacitive micromachined ultrasonic transducers," *IEEE Trans. Ultrason. Ferroelectr. Freq. Control*, vol. 52, no. 12, pp. 2270–2275, 2005.
- [2] A. Caronti, A. Savoia, G. Caliano, and M. Pappalardo, "Acoustic coupling in capacitive microfabricated ultrasonic transducers: Modeling and experiments," *IEEE Trans. Ultrason. Ferroelectr. Freq. Control*, vol. 52, no. 12, pp. 2220–2234, 2005.
- [3] G. G. Yaralioglu, A. S. Ergun, and B. T. Khuri-Yakub, "Finite-element analysis of capacitive micromachined ultrasonic transducers,"

- IEEE Trans. Ultrason. Ferroelectr. Freq. Control*, vol. 52, no. 12, pp. 2185–2198, 2005.
- [4] B. Bayram, M. Kupnik, G. G. Yaralioglu, O. Oralkan, D. Lin, X. Zhuang, A. S. Ergun, A. F. Sarioglu, S. H. Wong, and B. T. Khuri-Yakub, "Characterization of cross-coupling in capacitive micromachined ultrasonic transducers," in *Proc. IEEE Ultrasonics Symp.*, 2005, pp. 601–604.
 - [5] M. Buigas, F. M. Espinosa, G. Schmitz, I. Ameijeiras, P. Masegosa, and M. Dominguez, "Electro-acoustical characterization procedure for CMUTs," *Ultrasonics*, vol. 43, no. 5, pp. 383–390, 2005.
 - [6] O. Oralkan, B. Bayram, G. G. Yaralioglu, A. S. Ergun, M. Kupnik, D. T. Yeh, I. O. Wygant, and B. T. Khuri-Yakub, "Experimental characterization of collapse mode CMUT operation," *IEEE Trans. Ultrason. Ferroelectr. Freq. Control*, vol. 53, no. 8, pp. 1513–1523, 2006.
 - [7] A. Caronti, R. Carotenuto, and M. Pappalardo, "Electromechanical coupling factor of capacitive micromachined ultrasonic transducers," *J. Acoust. Soc. Am.*, vol. 113, no. 1, pp. 279–288, 2003.
 - [8] A. Nikoozadeh, B. Bayram, G. G. Yaralioglu, and B. T. Khuri-Yakub, "Analytical calculation of collapse voltage of CMUT membrane," in *Proc. IEEE Ultrasonics Symp.*, 2004, pp. 256–259.
 - [9] I. O. Wygant, M. Kupnik, and B. T. Khuri-Yakub, "Analytically calculating membrane displacement and the equivalent circuit model of a circular CMUT cell," in *Proc. IEEE Ultrasonics Symp.*, 2008, pp. 2111–2114.
 - [10] G. G. Yaralioglu, A. S. Ergun, B. Bayram, E. Haeggstrom, and B. T. Khuri-Yakub, "Calculation and measurement of electromechanical coupling coefficient of capacitive micromachined ultrasonic transducers," *IEEE Trans. Ultrason. Ferroelectr. Freq. Control*, vol. 50, no. 4, pp. 449–456, 2003.
 - [11] W. P. Mason, *Electromechanical Transducers and Wave Filters*. New York, NY: Van Nostrand, 1942.
 - [12] G. Caliano, A. Caronti, M. Baruzzi, A. Rubini, A. Iula, R. Carotenuto, and M. Pappalardo, "PSPICE modeling of capacitive micro-fabricated ultrasonic transducers," *Ultrasonics*, vol. 40, no. 1–8, pp. 449–455, 2002.
 - [13] A. Caronti, G. Caliano, A. Iula, and M. Pappalardo, "An accurate model for capacitive micromachined ultrasonic transducers," *IEEE Trans. Ultrason. Ferroelectr. Freq. Control*, vol. 49, no. 2, pp. 159–168, 2002.
 - [14] D. Certon, F. Teston, and F. Patat, "A finite difference model for CMUT devices," *IEEE Trans. Ultrason. Ferroelectr. Freq. Control*, vol. 52, no. 12, pp. 2199–2210, 2005.
 - [15] I. Ladabaum, X. Jin, H. T. Soh, A. Atalar, and B. T. Khuri-Yakub, "Surface micromachined capacitive ultrasonic transducers," *IEEE Trans. Ultrason. Ferroelectr. Freq. Control*, vol. 45, no. 3, pp. 678–690, 1998.
 - [16] A. Lohfink and P. C. Eccardt, "Linear and nonlinear equivalent circuit modeling of CMUTs," *IEEE Trans. Ultrason. Ferroelectr. Freq. Control*, vol. 52, no. 12, pp. 2163–2172, 2005.
 - [17] H. K. Oguz, A. Atalar, and H. Koymen, "Equivalent circuit-based analysis of CMUT cell dynamics in arrays," *IEEE Trans. Ultrason. Ferroelectr. Freq. Control*, vol. 60, no. 5, pp. 1016–1024, 2013.
 - [18] H. K. Oguz, S. Olcum, M. N. Senlik, V. Tas, A. Atalar, and H. Koymen, "Nonlinear modeling of an immersed transmitting capacitive micromachined ultrasonic transducer for harmonic balance analysis," *IEEE Trans. Ultrason. Ferroelectr. Freq. Control*, vol. 57, no. 2, pp. 438–447, 2010.
 - [19] X. Jin, O. Oralkan, F. L. Degertekin, and B. T. Khuri-Yakub, "Characterization of one-dimensional capacitive micromachined ultrasonic immersion transducer arrays," *IEEE Trans. Ultrason. Ferroelectr. Freq. Control*, vol. 48, no. 3, pp. 750–760, 2001.
 - [20] M. N. Senlik, S. Olcum, H. Koymen, and A. Atalar, "Radiation impedance of an array of circular capacitive micromachined ultrasonic transducers," *IEEE Trans. Ultrason. Ferroelectr. Freq. Control*, vol. 57, no. 4, pp. 969–976, 2010.
 - [21] H. Koymen, A. Atalar, E. Aydogdu, C. Kocabas, H. K. Oguz, S. Olcum, A. Ozgurluk, and A. Unlugedik, "An improved lumped element nonlinear circuit model for a circular CMUT cell," *IEEE Trans. Ultrason. Ferroelectr. Freq. Control*, vol. 59, no. 8, pp. 1791–1799, 2012.
 - [22] B. Bayram, E. Haeggstrom, G. G. Yaralioglu, and B. T. Khuri-Yakub, "A new regime for operating capacitive micromachined ultrasonic transducers," *IEEE Trans. Ultrason. Ferroelectr. Freq. Control*, vol. 50, no. 9, pp. 1184–1190, 2003.
 - [23] S. Olcum, Y. Yamaner, A. Bozkurt, H. Koymen, and A. Atalar, "Deep collapse operation of capacitive micromachined ultrasonic

transducers," *IEEE Trans. Ultrason. Ferroelectr. Freq. Control*, vol. 58, no. 11, pp. 2475–2483, 2011.

- [24] S. Olcum, Y. Yamaner, A. Bozkurt, H. Koymen, and A. Atalar, "An equivalent circuit model for transmitting capacitive micromachined ultrasonic transducers in collapse mode," *IEEE Trans. Ultrason. Ferroelectr. Freq. Control*, vol. 58, no. 7, pp. 1468–1477, 2011.
- [25] S. Timoshenko and S. W. Woinowsky-Krieger, *Theory of Plates and Shells*. New York, NY: McGraw-Hill, 1959.
- [26] A. Ozgurluk, A. Atalar, H. Koymen, and S. Olcum, "Radiation impedance of collapsed capacitive micromachined ultrasonic transducers," *IEEE Trans. Ultrason. Ferroelectr. Freq. Control*, vol. 59, no. 6, pp. 1301–1308, 2012.



Elif Aydoğdu was born in Ankara, Turkey, in 1982. She received her B.S. and M.S. degrees in electrical and electronics engineering in 2004 and 2007, respectively, from Bilkent University, Ankara, Turkey. She is currently working toward her Ph.D. degree in the same department, where she has been a research assistant since 2004. Her research interests included mechanical energy harvesting and magnetic resonance imaging, and currently she is working on modeling and design of CMUTs.



Alper Özgürlük was born in Kirikkale, Turkey, in 1990. He received his B.S. degree in electrical engineering in 2012 from Bilkent University, Ankara, Turkey. He is currently working toward his Ph.D. degree in the Department of Electrical Engineering and Computer Sciences at the University of California, Berkeley, CA. His current research interests include micromechanical filters, switches, and modeling of CMUTs.



Abdullah Atalar received his B.S. degree from the Middle East Technical University, Ankara, Turkey, in 1974, and his M.S. and Ph.D. degrees from Stanford University, Stanford, CA, in 1976 and 1978, respectively, all in electrical engineering. He worked at Hewlett-Packard Labs, Palo Alto, CA, in 1979. From 1980 to 1986, he was on the faculty of the Middle East Technical University as an Assistant Professor. In 1986, he joined Bilkent University as the chairman of the Electrical and Electronics Engineering Department and served in the founding of the department where he is currently a Professor. In 1995, he was a Visiting Professor at Stanford University. From 1996 to 2010, he was the Provost of Bilkent University. He is presently the Rector of the same university. His current research interests include micromachined devices and microwave electronics.

Prof. Atalar was awarded the Science Award of TUBITAK in 1994. He is a Fellow of IEEE and a member of Turkish Academy of Sciences.



Hayrettin Köymen received the B.Sc. and M. Sc. degrees from the Middle East Technical University (METU), Ankara, Turkey, in 1973 and 1976, respectively, and the Ph.D. degree from Birmingham University, UK, in 1979, all in electrical engineering. He worked as a faculty member in the Marine Sciences Department (Mersin) and Electrical Engineering Department (Ankara) of METU, from 1979 to 1990. Since 1990, he has worked at Bilkent University, where he is a professor. His research activities have included underwater

acoustic and ultrasonic transducer design, acoustic microscopy, ultrasonic NDT, biomedical instrumentation, mobile communications, and spectrum management.

Prof. Koymen is a fellow of IET (formerly IEE).